J Mater Sci (2012) 47:108–120
DOI 10.1007/s10853-011-5945-2

Optical and electrochemical properties of multilayer polyelectrolyte thin films incorporating spherical, gold colloid nanomaterials

Tran T. Doan · Robert W. Day · Michael C. Leopold

Received: 28 July 2011 / Accepted: 8 September 2011 / Published online: 27 September 2011

Abstract Polyelectrolyte multilayer (PEM) films incorporating various types of spherical, gold nanomaterials (NMs) were investigated to assess the existence of electrochemical and/or optical signal enhancement effects directly attributable to embedded NMs and the relationship of these effects to film structure and composition. Specifically, electrostatically assembled films of cationic poly-L-lysine (PLL) and anionic poly(4-styrene sulfonate) (PSS) incorporating one of four types of spherical, gold colloid NMs were constructed on 3-(aminopropyl)trimethoxysilane (3-APTMS)-modified glass substrates for optical studies or 11-mercaptoundecanoic (MUA)-modified gold electrodes for electrochemical studies. The NMs inserted into the PEM films include citrate-stabilized gold nanoparticles, thioctic acid-stabilized gold nanoparticles (TAS-NPs), MUA-modified monolayer protected gold clusters, and hollow gold nanoshells (Au-NSs). Optical sensitivity of the NM-embedded films, in terms of absorbance, surface plasmon band shifts, and the dependence of these optical responses on film thickness, varied depending on the type of NM within the film (e.g., TAS-NPs versus Au-NSs) but exhibited no corresponding electrochemical effects in the diffusional voltammetry of a ferricyanide redox probe. While not correlated to optical responses, the increased Faradaic current achieved during voltammetry at NM-embedded PEM films suggested that electrochemical effects of NMs were less dependent on the type of NMs and were, instead, more related to their location within the film and the electrostatic interactions built into the interfacial chemistry of the films. These results should prove useful for developing strategies constructing thin films with NMs that are specifically designed for optical or electrochemical sensing, taking full advantage of the signal enhancements provided by individual types of NMs.

Electronic supplementary material The online version of this article (doi:10.1007/s10853-011-5945-2) contains supplementary material, which is available to authorized users.

T. T. Doan · R. W. Day · M. C. Leopold (✉)
Department of Chemistry, Gottwald Center for the Sciences, University of Richmond, Richmond, VA 23173, USA
e-mail: mleopold@richmond.edu

Introduction

A number of different types of noble metal nanostructured materials have emerged in recent years, offering new insights to their unique optical and electrochemical properties. Both optical properties, like surface plasmon resonance spectroscopy and surface-enhanced Raman scattering, and electrochemical properties, like coulomb blockade behavior and quantized capacitance charging, are easily manipulated by varying core size, geometry, aspect ratio, composition, surface modification, and dielectric environment, ultimately offering greater control in bio- or chemo-detection schemes [1–8]. The usefulness of nanomaterials (NMs) as optical and electronic enhancers is allied by their versatility and, thus, is a common theme in many scientific explorations, particularly ones that implement film assemblies built on transparent substrates (e.g., glass, metal-oxides) or metallic electrodes that incorporate these different NMs in a systematic manner.

Some types of NMs are more optically or electrochemically interesting than others in that they promote a signal, either in terms of absorbance (optical) or current (electrochemical), enhancement. Spherical nanoparticles (NPs) remain one of the more widely studied sets of NMs in this respect. For example, Fermin and coworkers [9] have shown that adsorbing a monolayer of citrate-stabilized, spherical

gold nanoparticles (CS-NPs) onto an alkanethiol-modified gold electrode enhances the electron transfer (ET) rate compared to systems without adsorbed NPs. Optically, Sun and Xia [3] have demonstrated that spherical, hollow gold nanoshells (Au-NSs) offer enhanced plasmonic properties and sensitivity in detecting local environmental changes compared to their solid core NPs counterparts of similar sizes. Specifically, the surface plasmon band (SPB) of Au-NSs is subjected to impressive tunability over a spectral region from 600 to 1200 nm, achievable by modifying the Au-NSs' surface alkanethiolate peripheral layers and/or refractive index of the surrounding medium. In contrast, the SPB of spherical gold NPs is difficult to shift more than 20 nm through surface modifications [10–13].

The unique optical and electrochemical properties of these spherical NMs have prompted the study of their incorporation as functional components of sensing schemes. Investigations of this nature are often extensively focused on the architectures of ultrathin film assemblies. These functional hybrid devices sometimes feature NPs covalently adsorbed on electrode substrates via dithiols linkers. For example, electrochemical enhancement of protein monolayer electrochemistry is observed for dithiol-linked monolayer protected gold cluster (MPC) films that serve as an alternative adsorption platform to the traditional alkanethiolate self-assembled monolayer (SAM)-modified electrodes. These MPC systems show both a lack of traditional ET distance dependence through the film assembly [7, 13], as well as improved interfacial homogeneity that yield more uniform protein adsorption and optimized voltammetry compared to analogous SAM platforms [13, 14].

One of the most flexible and controllable methods to prepare nanostructured films employs electrostatic adsorption of charged colloidal NMs and polyelectrolyte (PE) layers [1, 2, 15–20]. First described in 1992 by Decher et al., these films received considerable attention because the electrostatic interaction between PE layers could be exploited as a linking mechanism [21]. Branching from their idea, research groups have effectively built NM-polyelectrolyte multilayer (PEM) films using a layer-by-layer assembly of alternating deposition of anionically or cationically modified MPC monolayers and their counter-ionic polymeric linkers to investigate the stability of an extensive range of functionalized and hybrid MPCs [16, 22]. Work by our own research group has reported a successful architecture of air stable multilayer films incorporating NMs by constructing multilayer polymeric bridges, specifically of alternating cationic poly-L-lysine (PLL) and anionic poly(4-styrene sulfonate) (PSS), between monolayers of NPs or NSs [1]. PEM-modified electrodes incorporating NMs used in electrochemical studies have shown faradaic current amplification of both surface-confined and diffusing electroactive molecules [19, 20]. These studies suggest that the NM-PEM films enhance ET dynamics by decreasing the charge-transfer resistance, a barrier usually introduced by commonly employed carboxylic acid alkanethiol surface modification that subsequently decrease electron tunneling probability. By varying position and density of embedded CS-NPs, distance dependence and interfacial electronic coupling between NPs have been identified as noteworthy factors when accessing enhancements of current or apparent ET kinetics [2]. Au-NSs incorporated into PEM films express enhanced optical properties that can be exploited as both reporters of their local environment and as detectors of molecular binding events on Au-NSs' interfaces, both of which are more sensitive than their solid core NP counterpart films [3, 18].

In this article, optical and electrochemical signal enhancements as the direct result of incorporating various types of spherical gold colloid NMs into PEM were investigated. From the literature, it is readily evident that there are numerous types and shapes of NMs each with a range of sizes, protective ligands, and composition (i.e., metallic versus carbon-based), making an exhaustive study of all NMs impractical for all intensive purposes. For our purposes here, we have intentionally limited our focus to a specific subset of NMs—spherical gold colloids differing in size, peripheral protective ligands, and structure (i.e., solid core versus hollow interior). The NMs used in this study include CS-NPs, thioctic acid-stabilized NPs (TAS-NPs), and 11-mercaptoundecanoic (MUA) functionalized MPCs (MUA-MPCs), and hollow Au-NSs. For optical investigations, NM-PEM films are confined on silanized glass slides and for electrochemical investigations, the films are assembled on SAM-modified gold electrodes. Their resulting optical and electrochemical properties are analyzed by ultraviolet–visible (UV–Vis) spectroscopy and cyclic voltammetry (CV), respectively. Optical variables taken into consideration to analyze NM enhancement include shifts of both absorbance at lambda maximum (λ_{max}) and localized surface plasmon resonance as a result of changes in the local environment. In turn, electrochemical variables consist of electrostatic interactions between electrochemical redox species probe and terminating layer of NS-PEM films and pH dependency on the layer-by-layer processing of weak PEs. While some of these materials have been previously shown to be related to certain signal enhancements, their relative effects within films have not been specifically examined nor have the factors that control the enhancement effects such as the location of the NMs within the films. More fully elucidating these factors and the relative intensity of the enhancements from embedded NMs is the focus of the following study.

Experimental procedure

Chemicals and materials

All chemicals were purchased commercially and used as received unless otherwise noted. PLL (MW > 30,000) and PSS (MW 70,000) polymer linkers were dissolved in chilled sodium phosphate buffer (8.8 mM, pH 8.5) to prepare 0.5 mM stock solution concentrations. Polymers dip solutions were made by diluting 500 μL of polymer stock solution into 8 mL of the same buffer. The ω-substituted alkanethiol modifying ligand, specifically MUA acid (Sigma-Aldrich), was used as 5 mM ethanol solution. All glassware was aqua-regia (3:1 HCl, HNO_3) cleaned and thoroughly rinsed with 18 MΩ ultrapure water (UP H_2O) before use.

Synthesis of CS-NPs

Procedures used to produce CS-NPs were developed and described in detail by Natan and coworkers [23–25]. In short, 1 mM $HAuCl_4$ aqueous solution was placed in a flask fitted with a reflux condenser and then heated to reflux with constant stirring. A 38.8 mM sodium citrate aqueous solution was rapidly added, resulting in color transitions from light yellow to colorless and to burgundy (wine red). After 10 min of reflux, the solution was removed from heat and cooled to room temperature with stirring. The product was vacuum filtrated with a 0.8 μm Gelman membrane filter and stored in the dark. Characterization of CS-NPs by UV–Vis spectroscopy (Agilent 8453 Photo Diode) and transmission electron microscopy (TEM) (Fig. 1a) showed the characteristic SPB at 520 nm and an average diameter of $\sim 10.32 \pm 2.73$ nm.

Synthesis of TAS-NPs

TAS-NPs were created from using the aforementioned CS-NPs as a starting material with a method previously described by Chen and coworkers [26]. Immediately after synthesis, the pH of the CS-NP solution was adjusted to basic conditions (pH 11) using aliquots of 0.5 M sodium hydroxide to ensure charge retention during stabilization with thioctic acid. A molar quantity of thioctic acid to $HAuCl_4$ was added, and resulting solution was stirred overnight in the dark. The solution was then centrifuged for 20–30 min at ~15,900 rpm and 10 °C (Sorvall RC-5B Refrigerated Superspeed). The supernatant was decanted, and resulting solid was reconstituted in UP H_2O to create a burgundy (wine red) solution that is then stored in the dark. UV–Vis spectra and TEM imaging of TAS-NPs (Fig. 1b) expressed similar SPB and average core size, respectively, as CS-NPs but possess significantly greater stability [27].

Synthesis of MUA-stabilized Au-NSs

Hollow Au-NSs were prepared in the dark using a procedure outlined by Xia et al. where silver NPs (Ag-NPs) act as sacrificial templates for Au-NSs. For a typical Ag-NP synthesis [28], 10.0 g polyvinylpyrrolidone (PVP) (0.182 mmol) and 0.400 g $AgNO_3$ (2.35 mmol) were both completely dissolved in 50 and 15 mL of ethylene glycol (EG), respectively. Upon adding $AgNO_3$-EG to PVP-EG, the solution was refluxed for 12 h in an oil bath at 120 °C with stirring, ultimately resulting in color shifts from colorless to yellow to brown and finally to green–brown with a metallic tint. Subsequently, the solution was cooled to room temperature, washed with 200 mL acetone, and centrifuged for 20 min at 10,000 rpm and 10 °C. The clear yellow supernatant was decanted, and the dark brown pellet was re-dissolved in UP H_2O. After a second centrifugation, the final product was reconstituted in 100 mL UP H_2O and stored in the dark. UV–Vis spectroscopy and TEM characterization of Ag-NPs (Supplementary Material) showed a defined SPB at 410 nm and an average diameter of 24.39 ± 4.62 nm.

For Au-NSs synthesis, a dilute solution of the Ag-NPs (1:20 mL stock Ag-NPs to UP H_2O) was heated to reflux with constant stirring at 250 rpm. After 10 min of refluxing, 1 mM $HAuCl_4$ was added dropwise very slowly. The addition of $HAuCl_4$ initiates a replacement reaction featuring the simultaneous deposition of Au via the reduction of Au^{3+} and dissolution of Ag metal sacrificial templates via oxidation [11]. The progress of the replacement reaction can be monitored with UV–Vis spectroscopy where the SPB of the Ag-NPs at 410 nm slowly disappears with the steady emergence of the SPB of the Au-NSs at ~680 (Supplementary Material). With the establishment of the Au-NSs' SPB, the addition of Au salt was halted, and the solution was allowed to reflux for 20 min before cooling to room temperature and centrifuging for 15 min at 10,000 rpm and 10 °C. After centrifugation, the supernatant was decanted, and the pellet was resuspended in UP H_2O, a process repeated at least two more times, until a final dark blue pellet was re-dissolved in 10 mL of UP H_2O to create a royal blue solution that is then stored in the dark. The Au-NSs were stabilized with MUA by stirring 1:500 volume ratio of 5 mM MUA ethanol solution to "as-prepared" Au-NSs for 5 h. The pH was adjusted to 8 by adding 0.5 mM NaOH dropwise to retain electrostatic repulsion (i.e., prevent aggregation) between Au-NSs and terminal carboxylic acids during centrifugation for 30 min at 10,000 rpm. The resulting pellet was reconstituted in UP H_2O. TEM characterization (Fig. 1c) determined an

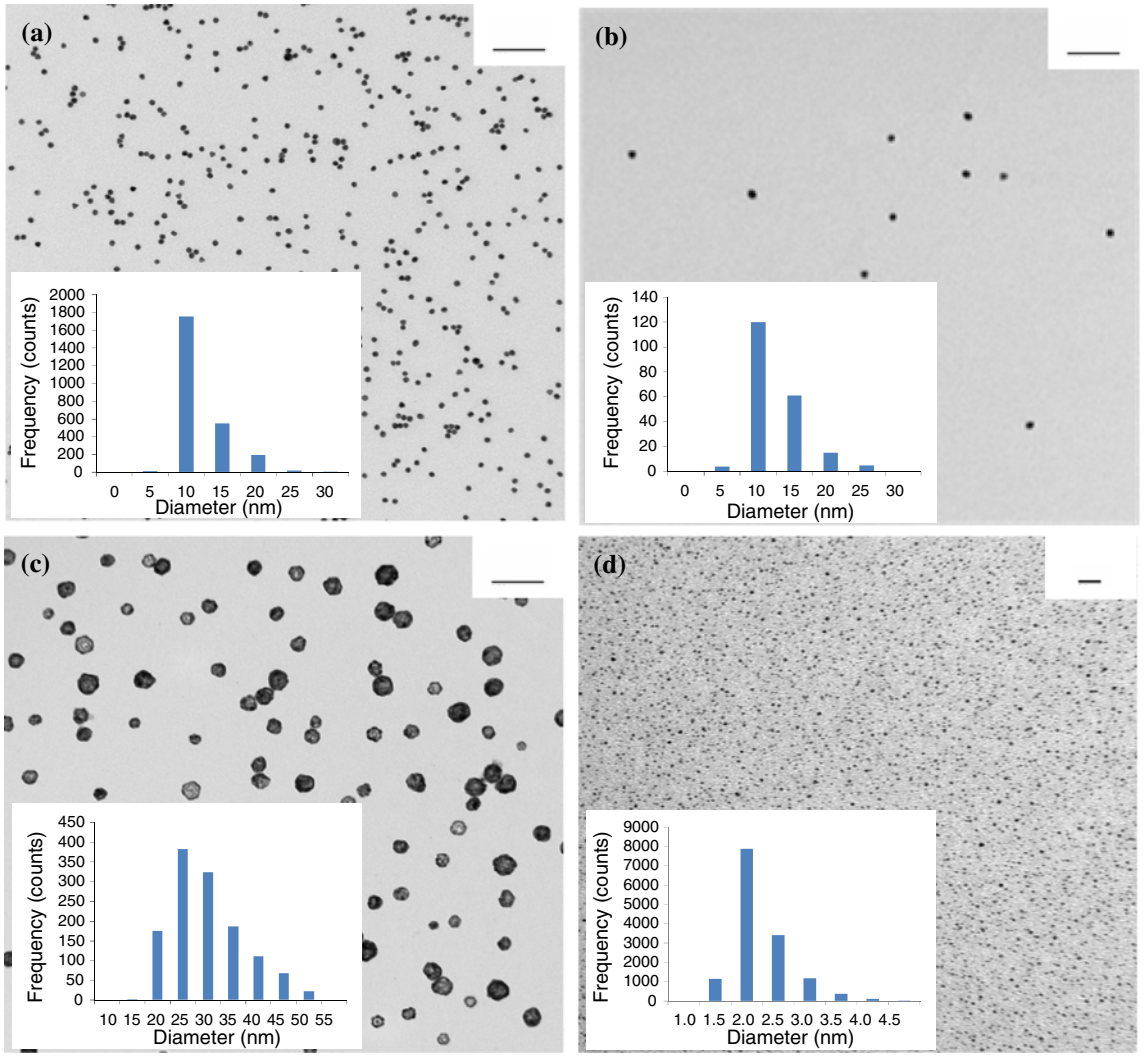

Fig. 1 Typical transmission electron microscopy (TEM) images of aqueous **a** CS-NPs, **b** TAS-NPs, **c** Au-NSs, and **d** MUA-MPCs (suspended in ethanol) taken at ×40000, ×50000, ×40000, and ×100000 magnifications, respectively. *Insets* display the histogram analysis of core size determined from TEM imaging. The *bars* in the *upper right corners* of the images signify 100 nm for (**a**–**c**) and 20 nm for (**d**)

average diameter of the NSs was ∼27.24 ± 7.13 nm and was consistent with literature reports of these NSs [1].

Synthesis of MUA-MPCs

Hexanethiolate-protected MPCs were synthesized using a modified Brust reaction [29, 30] from Au salt $HAuCl_4$, previously crystallized from aqua-regia reflux of 99.99% Au shot. In brief, aqueous $HAuCl_4$ was treated with tetraoctylammonium bromide in toluene to phase-transfer the Au ions from the aqueous to the nonaqueous layer. A mole ratio of 2:1 hexanethiol to Au was added to the separated nonaqueous layer, and the resulting solution was stirred for 30 min during which color transitions from reddish orange to a pale yellow solution were observed. Chilled aqueous sodium borohydride (0.5 M) was added to the flask at 0 °C, immediately producing a thick black solution of MPCs. This solution was stirred overnight, separated, and rotary evaporated to near dryness before the MPC material was precipitated with acetonitrile (overnight) and collected in a medium porosity glass frit. The average core diameter, determined by TEM analysis (Fig. 1d), was 1.96 ± 0.45 nm with an average composition of $Au_{225}(C6)_{75}$ and agreed with literature [7, 13, 14].

MPCs were functionalized with MUA according to a previously reported place-exchange technique [7, 31]. To functionalize, MPCs and MUA (1:2 MUA to hexanethiol mole ratio) were co-dissolved in tetrahydrofuran and stirred for 72 h before the MUA-functionalized MPCs were precipitated (overnight) with acetonitrile and collected in a medium porosity glass frit. On average, the composition of the functionalized MPC was determined to

be $Au_{225}(C6)_{45–46}(MUA)_{29–30}$ or approximately 40% surface-bounded MUA by NMR analysis of samples after iodine-induced oxidative decomposition, as previously reported [7, 30].

Film assembly

Various NMs were incorporated within PE films assembled either on Piranha-cleaned glass slides [*Warning! Piranha solution (2:1) conc. H_2SO_4 to H_2O_2 reacts violently with organic material, handle with extreme caution!]* or gold electrodes mounted in electrochemical sandwich cells as previously described [7, 13, 14, 32]. For optical investigations, the glass slides were first silanized with 3-(aminopropyl)trimethyloxysilane (3-APTMS) (Sigma-Aldrich) before exposing them to NMs for 1 h [1, 27, 33]. The slides were then immersed in alternating PLL and PSS dip solutions for 30 min each with copious rinsing with UP H_2O in between layers. To monitor film growth, individual slides were placed in quartz cuvette filled with UP H_2O, and UV–Vis spectra were taken after each added layer. As expected,[1,23–25] there is a slight red shift upon immobilizing the NMs to the substrate and it should be noted that even though the parent bulk solutions are colorful, these thin films, having only a single layer of NMs, appear transparent with only a very slight tint of color (Supplementary Material). The PEM films used in electrochemical investigations were assembled according to previously described procedures [2, 27]. The gold electrodes served as the working electrode and were electrochemically cycled in a solution of 0.1 M sulfuric acid and 0.01 M potassium chloride [2, 7, 13, 14, 34]. The clean gold was then treated with 5 mM MUA ethanolic solution for ~48 h to form a carboxylic acid-terminated SAM. The PE layer-by-layer film was assembled by immersing the gold in alternating PLL and PSS dip solutions for 30 min each before exposing the gold to aqueous NMs (CS-NPs, TAS-NPs, or Au-NSs) or MUA-MPCs ethanolic solution (1 mg/1 mL) for 1 h with copious washing in between layers.

Electrochemistry

CV was performed using CH Instruments potentiostats (Model 650A or 610B) fitted with both a low current amplifier and a Faraday cage. The electrochemical sandwich cell has been extensively used and described by our laboratory, and features a Ag/AgCl (saturated KCl) reference electrode (Microelectrode, Inc), a platinum wire (Sigma-Aldrich) counter electrode, and an evaporated gold substrate (Evaporated Metal Films) as a working electrode defined by a Viton *o*-ring with a geometric surface area of 0.32 cm^2. Solution voltammetry was performed on 5 mM potassium ferricyanide ($Fe(CN)_6^{3-/4-}$) in 0.5 M KCl supporting electrolyte and was scanned within the potential window of −0.2 to 0.6 V at 100 mV/s versus Ag/AgCl.

Transmission electron microscopy and image J analysis

TEM images of NMs were obtained by a JEOL 1010 microscope operating at 80–100 kV. Aqueous NMs and dry MPC materials (dissolved in toluene) were drop-casted onto 400 mesh copper grid coated with Formvar (Electron Microscopy Sciences). Image analysis was performed using Image J program to determine average core size of the samples. The program evaluated the area measurements of individual NMs detected in the TEM images from pixel value statistics of user-specified parameters, which included intensity threshold (varied with image), minimum core size (~50-infinity), circularity (0.00–1.00), and distance in pixels (0). The correlated NMs' diameters were calculated from the program's measured areas ($pixel^2$) in which extraneous, exceedingly large and small values were disregarded as inaccurate contributions to average core diameters. From these computed diameters, histograms were created to determine the average core size and its standard deviation and to observe the range of the samples' diameters.

Results and discussion

Figure 1 shows TEM imaging and analysis of the different types of colloidal gold NMs investigated in our study including CS-NPs, TAS-NPs, Au-NSs, and MUA-MPCs. All of these NMs are spherical, but differ in either their size, protective ligand, or structural composition. These various gold colloids were incorporated into two general schemes of film assemblies: (1) anchoring the NMs onto a modified substrate before adding alternating PLL-PSS PE layers on top of them or (2) adsorbing the NMs at the film/solution interface of an existing film of alternating PLL-PSS PE layers. Both of these film schematics take advantage of electrostatic interactions between NMs, PE layers, and modified substrates to dictate the layering system. The resulting optical and electrochemical properties of these NM-embedded films were analyzed by UV–Vis spectroscopy and CV, respectively.

Analysis of optical properties of thin films with embedded NMs

Each of the NMs investigated in this study exhibits a signature response in the UV–Vis spectrum, most notably a SPB with a distinct λ_{max} value (Fig. 2). CS-NPs and TAS-NPs share similar SPB, featuring λ_{max} at ~520 nm. This similarity is expected given that CS-NPs serve as

template for the TAS-NPs, which are produced via thiol exchange reaction (i.e., they share the same metallic core and differ only in peripheral protective ligands). TAS-NPs are included in our study as an alternate form of CS-NPs, differing only in protective ligand (citrate versus thioctic acid), because prior study has shown that they are significantly more stable (i.e., resistant to aggregation) as both the as-prepared product and as part of a PEM film [27]. The signature SPB λ_{max} values of Ag-NPs and Au-NSs, ~410 and ~680 nm, respectively, are in excellent agreement with literature values [1, 3, 11]. Monitoring the extent of changes to these characteristic SPBs provides for evidence on the NMs' ability to detect their local environment. As a result, optical sensitivity of NMs can be investigated by incorporating them into various architectures of PEM films as a precursor for using these materials in sensor design.

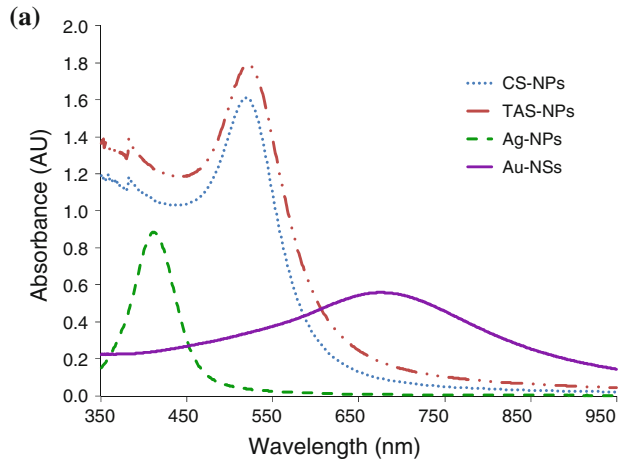

Fig. 2 **a** UV–Vis spectra of as-prepared aqueous NMs, including CS-NPs, TAS-NPs, Ag-NPs, and Au-NSs, taken immediately after synthesis. Ag-NPs are not gold-based like other aforementioned NMs but they serve as templates for Au-NSs, and thus their UV–Vis spectra are useful to confirm the presence of Ag-NPs. **b** Digital photographs of cuvettes containing bulk solutions of NMs: (*left to right*) CS-NPs (*wine red*), TAS-NPs (*wine red*), MUA-MPCs (*brown*), Ag-NPs (*yellow*), and Au-NSs (*blue*). Note: As-prepared MUA-MPCs, with an average core diameter of 1.96 ± 0.45 nm, do not express a defined SPB peak, and their UV–Vis spectrum is not displayed. (Color figure online)

In order to access their optical properties of films constructed with the different NMs, each type of material is incorporated into a film according to Scheme 1. That is, a monolayer of NMs is first anchored onto glass slides pretreated with 3-APTMS, so that the cationic amine group interacted electrostatically with the anionic protective groups of the specific NMs. Upon initial immobilization of the materials onto the substrate, there is a slight red shift of the SPB compared to solution spectra (Supplementary Material). Film growth is then accomplished by exposing the NM-modified glass slide to alternating cationic PLL and anionic PSS, totaling up to 25 PE layers. The effects of embedding the different colloidal materials within thin polymer films are investigated by UV–Vis spectroscopy. Incremental changes to the optical properties such as SPB position and absorbance as more PE layers are added are recorded and reveal information regarding the NMs' sensitivity to their local environment.

One of the more interesting optical property comparisons emerging from studies of films built according to Scheme 1 are those films incorporating TAS-NPs versus those assembled with Au-NSs in that they deliver drastically different optical responses within the PEM films. As the TAS-NP films are assembled with successive PE layers, the SPB distinctive for the TAS-NPs is observed to steadily increase in absorbance at λ_{max} while experiencing only a very slight (~5 nm) red shift as seen in Fig. 3a. In stark contrast to these results are the observations of the same experiment carried out with Au-NS-anchored films. In this scenario, the shell's characteristic SPB exhibits only a slight increase in absorbance at λ_{max} but reacts to the same PE layering by showing a much more substantial red shift (~23 nm) compared to the NP-based film (Fig. 3b). This significant difference in the optical sensitivity of the TAS-NPs and Au-NSs toward the PE ad-layers is easily observed by comparing narrower wavelength windows surrounding λ_{max} of the SPB for each set of experiments (Fig. 3, insets).

The difference in optical sensitivity enhancement, in terms of magnitude of red shift and absorbance at λ_{max}, is significant between the films built with NSs versus NPs. As with other types of enhancement achieved with NMs in the literature [1, 2, 6, 15, 25, 27, 33, 35, 36], there is often associated distance dependence of the effect. That is, the increased sensitivity of these materials for their local environment is observed only under specific condition or a distinctive distance. In this case, with the layering of PE over the monolayers of the two types of NMs, both the drastic differences in sensitivity as well as the different distance dependencies of the effect are clearly observed. Figure 4 shows these comparisons effectively, including a tracking of the percent change in the maximum absorbance (Fig. 4a) and red shift of λ_{max} (Fig. 4b) for the localized

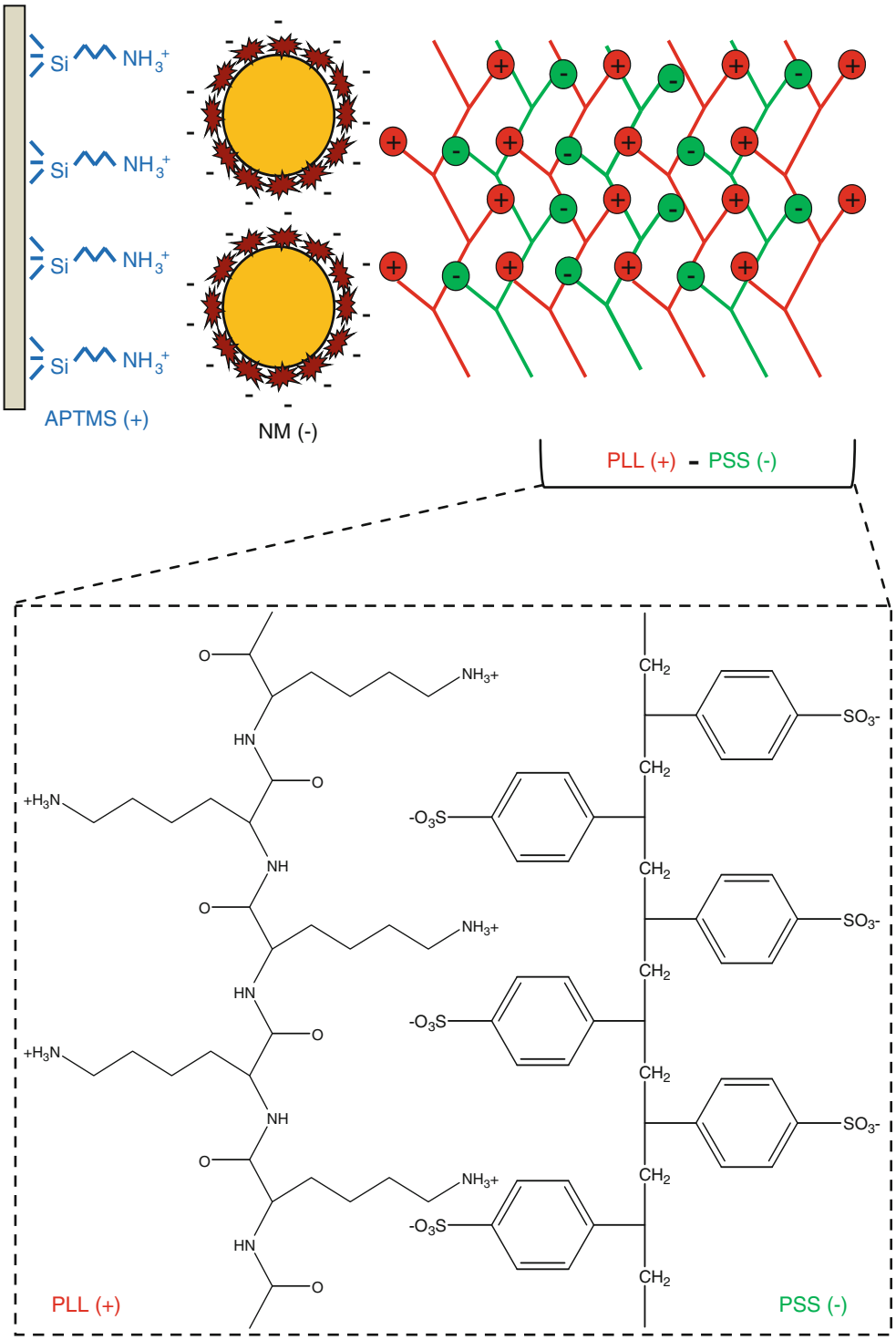

Scheme 1 Schematic of a typical film assembled for optical investigations. These films are composed of a negatively charged NM monolayer and alternating electrostatic PE layers mounted on a 3-APTMS-modified slide. The number of PE layers is not limited to the number displayed in the figure. The types of PE layers used include cationic PLL and anionic PSS (*Inset*). Similar films can be assembled with all the NMs studied

surface plasmon resonance signal of the TAS-NPs versus the Au-NSs. Figure 4a tracks the changes in absorbance at λ_{max} as a percent change of the original absorbance with increasing PE layers, providing a more quantitative comparison of the notably different optical responses between the two materials. Here, the percent change in absorbance at λ_{max} of the SPB for the NPs experiences a sharp increase ($\sim$30% increase) for the first 10–12 PE layers added while the SPB for the NS films increases only sparingly over the course of adding 25 PE layers ($\sim$10% increase). In terms of specific distance dependence, the TAS-NP-based films exhibit red shift that begins to plateau at 5–6 nm after less than 10 PE layers (5 bilayers) whereas the Au-NS-based films experience significant red shifting with increasing PE

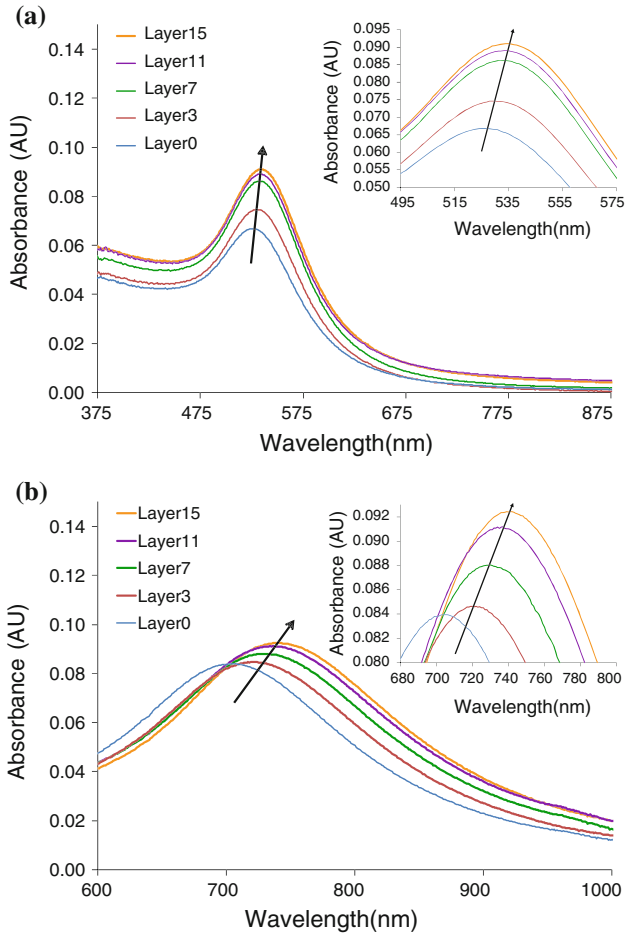

Fig. 3 Absorbance spectra of PE multilayered films built according to the Scheme 1 with embedded **a** TAS-NPs and **b** Au-NSs on 3-APTMS-modified slides and measured in NP H_2O. *Insets* display the smaller spectral window around λ max of the surface plasmon band (SPB)

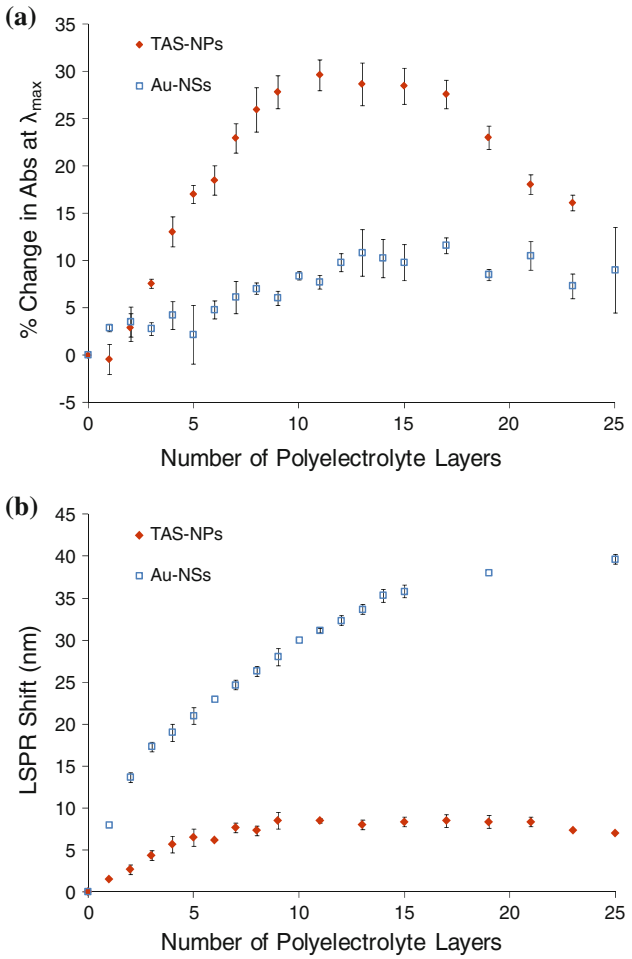

Fig. 4 Tracking **a** the percent change in the maximum absorbance and **b** the red shift of the localized surface plasmon resonance (LSPR) for films assembled via Scheme 1 on glass slides with TAS-NPs versus Au-NSs. Note: In some cases, the *error bars* are smaller than the data markers

ad-layers up to approximately 20 ad-layers (10 bilayers) before leveling out with a maximum red shift of nearly 40 nm (Fig. 4b). Multiple prior studies on the thickness of PE films [20, 40, 41] estimate that a single layer of similar PE in the presence of supporting electrolyte at comparable pH is approximately 0.64 nm per PE layer, suggesting that the NP and NS embedded films in our study express optical shifts in response to PE layer out to thicknesses of 6.4 and 12.8 nm, respectively.

The enhanced sensitivity of the NSs' optical response toward PE layering and the expanded distance of this effect compared to films with NPs is even more impressive if prior results on these materials are considered [1, 3, 6, 16]. Indeed, this general phenomenon has been observed before with the spectroscopy of NP and NS in solution that have been modified with increasing chainlengths of alkanethiol protecting ligands. These solution experiments reiterate the same sensitivity difference seen in our study with NSs showing a systematic and substantial red shift (up to 45 nm) upon modification with longer chainlength alkanethiols as compared to a red shift of only up to 8 nm for similar experiments with NPs. What is striking about the current result, given the optical shift is considered to largely attribute to changes in the local dielectric environment [1, 3, 37], is that the NS films remain notably sensitive to PE layering in spite of their original MUA coatings being present. Spectroscopy of films constructed with embedded CS-NPs showed consistent results with the films containing TAS-NPs (Fig. 3a) in that the predominant effects were an increase in λ_{max} absorbance coupled with a minor red shift (Supplementary Material). In addition, spectra of films with CS-NPs sometimes showed signs of aggregation consistent with the known stability of CS-NPs versus TAS-NPs (i.e., absorbance shoulder peaks emerging at ~620 nm) (Supplementary Material) [27]. Spectroscopy of films with MUA-MPCs revealed no significant SPB that

could be used to make a similar comparison to the other materials (not shown). Taken collectively all of these results, along with prior work, suggest a significant and persistent gain in optical sensitivity when hollow NSs are employed over solid core NPs in thin films with potential sensing application.

Analysis of electrochemical properties of thin films with embedded NMs

NMs embedded into thin film assemblies at gold electrodes have been shown to produce different electrochemical enhancements, including improved electronic coupling between particles [2], diminished ET distance dependence [7, 13], and lowered charge-transfer resistance [19, 20]. Given the significant optical enhancements observed in the aforementioned films, it follows to initiate our electrochemical study with systems most similar to the optical system depicted in Scheme 1. More specifically, for electrochemical experiments, MUA-modified gold electrodes are subsequently modified with a single layer of PLL to act as a cationic bridge between the SAM and the NMs [38]. After anchoring the NMs, PEMs are assembled as in previous optical experiments (Fig. 5a). In an attempt to establish a film system that possesses both electrochemical and optical enhancements, a parallel experiment similar to that shown in Figs. 3 and 4 was conducted with films of TAS-NPS or Au-NSs with seven overlying PE layers. These films correspond to the point in the optical experiments where the NP system optical response had reached a plateau and the NS system was still highly responsive in terms of both shift and absorbance maximum (Fig. 4). If the NS system has an inherent corresponding electrochemical effect, we would observe an effect with the NS system and not with the NP system.

The CV of a common solution redox species, $Fe(CN)_6^{3-/4-}$, is employed to assess the presence or absence of electrochemically enhanced behavior at NM-PEM film systems. The voltammetry of the $Fe(CN)_6^{3-/4-}$ probe is recorded at various stages of each film construction, examples of which are shown in Fig. 5b. Typical blocking behavior of long-chained alkanethiols SAM-modified electrode is observed with solution $Fe(CN)_6^{3-/4-}$ as compared to that of bare gold. In addition to the significant blocking of the electrode caused by the SAM, the complete disappearance of $Fe(CN)_6^{3-/4-}$ voltammetry is also likely assisted by electrostatic repulsion between the carboxylic acid end groups of the MUA-SAM and anionic $Fe(CN)_6^{3-/4-}$ species [19, 20]. As the films are further assembled with PEM and NMs, this initial completely blocked ("flatline") response of the probe the SAM, the anchoring layer of all the films, becomes paramount, as any voltammetric behavior observed beyond this blocked

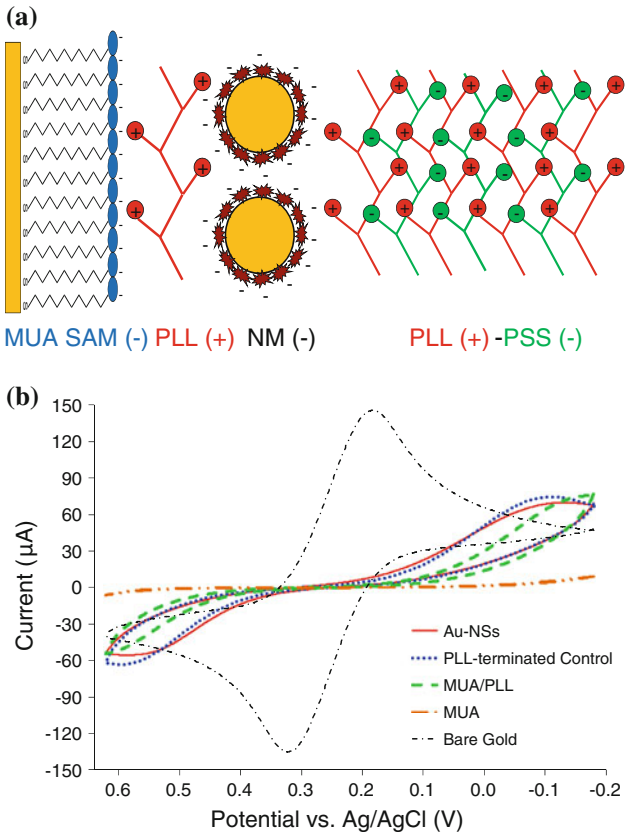

Fig. 5 **a** Schematic of a film constructed for electrochemical investigation adapted from Scheme 1 of a MUA-SAM-modified gold electrode, a PLL anchoring PE layer, negatively charged NM, and 7 alternating PLL and PSS layers; **b** Cyclic voltammetry (CV) of 5 mM ferricyanide ($Fe(CN)_6^{3-/4-}$) in aqueous 0.5 M KCl supporting electrolyte at 100 mV/s at bare gold, PLL MUA-SAM, MUA-SAM-modified gold, and PSS-terminated PEM films with and without (control) embedded Au-NSs. The results are representative of films with embedded CS-NPs, TAS-NPs, and MUA-MPCs with the latter expressing slightly more blocking behavior than the other NMs (Supplementary Material)

response can be considered an electrochemical enhancement. This concept is further illustrated with the addition of the single anchoring layer of cationic PLL onto the MUA-SAM (Fig. 5a), which causes a slight increase of faradiac response, attributed to the closer approach of the $Fe(CN)_6^{3-/4-}$ to the positively charged interface.

As previously mentioned, the initial PLL layer serves to anchor the various NMs to the interface before embedding them under PEMs. The $Fe(CN)_6^{3-/4-}$ voltammetry at these films incorporating NMs is then directly compared to the same films without NMs (control). A representative set of result for this type of comparison with Au-NS-embedded films is shown as part of Fig. 5b. The CV of $Fe(CN)_6^{3-/4-}$ at films with and without embedded Au-NSs show very little difference, no enhancement of any significance, and voltammetry typical of a diffusing species at a blocked electrode. Similar results (Supplementary Material) are

achieved with all the other NMs tested in this scheme (TAS-NPs, CS-NPs, and MUA-MPCs) suggesting that, with this general film geometry (Scheme 1), there is no film that clearly exhibits both an optical and electrochemical enhancement from the embedded NMs. Given the lack of electrochemical enhancement observed with the aforementioned films, experiments were designed to explore the properties of NM-embedded films where the NMs were incorporated at the film–solution interface rather than directly at the SAM layer of the modified electrode. That is, MUA-SAM-modified electrodes were treated with alternating layers of PE before ultimately terminating the entire assembly with the attachment of one of the four types of NMs (Scheme 2). As in the other experiments, $Fe(CN)_6^{3-/4-}$ voltammetry was measured at each stage of the film assembly, including completed films with and without (control) NMs at the interface. The control assemblies were films where the last PE layer in the assembly was either a sixth layer of anionic PSS or a seventh layer of cationic PLL. In all cases, however, the voltammetry of anionic $Fe(CN)_6^{3-/4-}$ at the negatively charged MUA-SAM displays complete blocking behavior that is notably improved once the first layer of positively charged PLL is attached. This result, which was highlighted in Fig. 5b, reiterates the sensitivity of the redox probe toward interfacial coulombic interactions and was consistently observed throughout all of the experiments. As such, it has been purposely omitted from subsequent voltammetry comparisons for greater clarity of presentation. Given the established repulsion of $Fe(CN)_6^{3-/4-}$ from negatively charged film interfaces, it follows then that complete blocking behavior would also be expected from a control film terminated with PSS or an experimental film with anionic NMs at its interface. This result is indeed observed at the PSS-terminated control film as the voltammetry of $Fe(CN)_6^{3-/4-}$ at the film matches exactly to that at a MUA-SAM (Fig. 6a). It is expected that the addition of anionic NMs via an additional cationic bridging lay of PLL would also elicit complete blocking in that (1) the interface remains negatively charged for electrostatic repulsion of $Fe(CN)_6^{3-/4-}$ and (2) the additional PE layer and NM make the film assembly notably thicker, a parameter known to further limit the probe's access to the electrode and slow ET kinetics [19, 20, 39]. Yet, as seen in Fig. 6a, the result of attaching, for example, negatively charged Au-NSs to the film assembly via the PLL bridge is significantly enhanced voltammetric activity that is well above the levels of the PSS control film and the MUA-SAM, a result that contradicts both expectations. Similar results were observed with films constructed with the other types of NMs as well, including voltammetric enhancement at films with the well insulated MUA-MPCs (Supplementary Material).

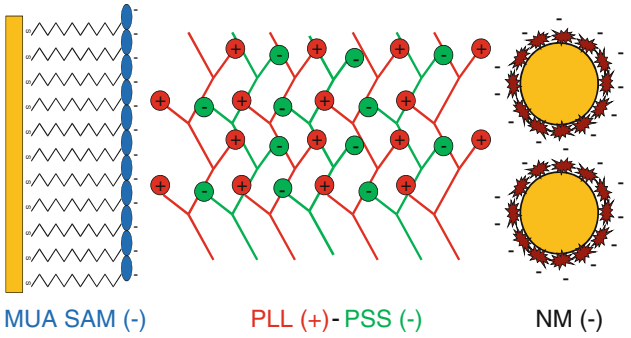

Scheme 2 Alternate schematic of a film assembled for electrochemical experiments with a MUA-SAM on a gold electrode, 7 alternating PLL and PSS PE layers, and terminated with a monolayer of negatively charged NMs at the solution interface

In a similar experiment, $Fe(CN)_6^{3-/4-}$ voltammetry was assessed at a control film (no NMs) where the final layer of PE was cationic PLL. As expected (Fig. 6b), the voltammetry of $Fe(CN)_6^{3-/4-}$ at the control film improved greatly compared to the MUA-SAM because of the now favorable interfacial electrostatics (i.e., an anionic redox probe at a cationic solution/electrode interface). The addition of any of the NMs, in this example the Au-NSs (Fig. 6b), to the film assembly was expected to diminish the observed voltammetry by introducing an unfavorable electrostatic interactions or probe/interface repulsion. Surprisingly, the voltammetry at the Au-NS-PEM films was largely unchanged from the control film, suggesting that the Au-NSs are indeed inducing an electrochemical enhancement that, to some extent, can overcome propensity for electrostatic repulsion of the $Fe(CN)_6^{3-/4-}$ probe. This result was observed for films incorporating the other types of NMs as well (Supplementary Material).

A clear implication of these electrochemical studies is the critical nature of coulombic interactions within the NMs-PEM films as well as at the solution interface. To this point, manipulation of electrostatic properties of a film is accomplished via specific alteration of different PE terminal layers or introduction of anionic NMs (Fig. 6a, b), strategies with significant impact on the electrochemical response at the films. The importance of coulombic interactions with these systems also suggests that the observed results may be strongly contingent on the electrostatic nature of the probe or pH. Studying the same films with alternative redox probes such as cationic ruthenium hexamine ($Ru(NH_3)_6^{2+/3+}$) or neutral hydroxylmethyl ferrocene did not result in the complete blocking of electroactivity at the SAM stage of the films (results not shown) as was seen with the $Fe(CN)_6^{3-/4-}$ results presented previously. Thus, in these systems, while it is clear electrostatic interactions are playing a significant role, a direct observation of enhancement remains somewhat ambiguous.

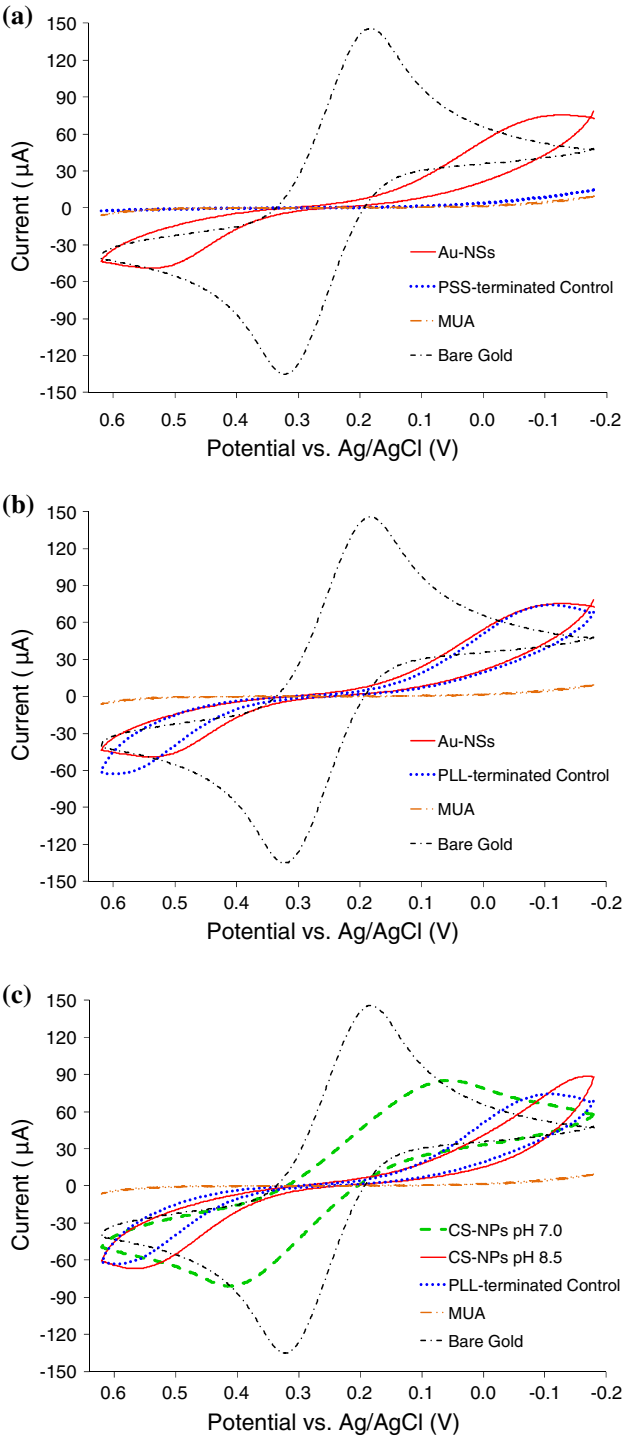

Fig. 6 Cyclic voltammetry (CV) of 5 mM ferricyanide ($Fe(CN)_6^{3-/4-}$) at PEM-modified electrodes with and without embedded NMs at the solution interface (Scheme 2); **a** Voltammetry at bare gold, MUA-SAM-modified gold, and PSS-terminated PEM films with and without (control) embedded Au-NSs; **b** Voltammetry at bare gold, MUA-SAM-modified gold, PLL-terminated PEM films with and without (control) embedded Au-NSs. These representative CV results are consistent for films incorporating CS-NPs and MUA-MPCs as well. In contrast, CV results at films incorporating TAS-NPs show slightly increased blocking behavior (Supplementary Materials); **c** Voltammetry at assembled films with embedded CS-NPs, constructed with PE dipping solutions at either pH 7.0 or 8.5, are compared. Also shown are the voltammetry at bare gold, MUA-SAM, and PLL-terminated control films

An alternative system to learn about coulombic interactions within films of this nature is to assemble an analogous film with opposite electrostatic properties. That is, gold modified with 11-amino-1-undecanethiol (Dojindo Molecular Technologies) creates a cationic interface instead of the anionic MUA interface. It is subsequently modified in the same manner as other films only with alternating layers of PSS(−) and PLL(+) before terminating with embedded NMs. Probing this system as it is assembled with an oppositely charged probe, $Ru(NH_3)_6^{2+/3+}$ as opposed to $Fe(CN)_6^{3-/4-}$, results in voltammetry that shows increasing irreversibility (i.e., negatively shifted $E_{p,c}$) in accordance with expected coulombic attraction/repulsion between the probe and the various interfaces, including abrupt movement of $E_{p,c}$ toward more positive potentials upon the addition of Au-NSs at the film interface (Supplementary Material).

In an effort to explore the effects of pH on film assembly and electrochemical enhancement, CS-NPs were incorporated at the interface of PEM films (Scheme 2) where the PE dip solutions used to form the film are held at either a pH of 7.0 or 8.5 before measuring the voltammetry of $Fe(CN)_6^{3/4-}$ at the film. The results of these experiments, depicted in Fig. 6c, show electrochemical enhancement of the signal at films formed from the pH 7 dipping solutions and a more diminished signal at the film formed from pH 8.5 dipping solutions. It has been suggested by Rubner and coworkers that the use of solutions of weak PE in the pH range of 7.5–9.5 result in multilayer films of notably higher thickness and increased charge-transfer resistance whereas those formed from solutions with a pH range of 6.0–7.5 are considerably less thick [40]. The results observed here are consistent with Rubner's findings in that the higher pH yields thicker films which will diminish the signal of a solution redox species, a well-known phenomena in the literature [40, 41] while the thinner pH 7 film will produce greater or enhanced electrochemical activity (Fig. 6c).

Conclusions

A systematic study of PEM films with various types of colloidal gold NMs built into their architectures was undertaken to study if the NP incorporation resulted in significant optical and/or electrochemical signal enhancements and identify factors that contribute to these effects. The cumulative results of this study suggest that while no one film structure or specific NM yields a film that is both electrochemical and optically enhanced, there are notable trends in both responses that should allow for more targeted design of NM hybrid thin films with potential sensing

applications. The spectroscopy of the NM-embedded films in this study indicates that the mere presence of any of the metallic NMs within the PEM film structure initiates a unique optical response attributable to a change in the NMs' local environment or dielectric field. While this optical effect is present regardless of the type of NMs used, its magnitude, effective distance, and nature can differ rather drastically depending on the type of NMs in the film. Most notably, Au-NS-embedded films display a red shift of significant magnitude of the SPB compared to an increase in maximum absorbance for TAS-NPs. Moreover, the greater sensitivity of the NS based films is also observed to be effective over a greater thickness of PEM film. The significantly different sensitivity of the hollow particles compared to their solid counterparts is consistent with solution studies on these materials [1] and is likely due to the fact that the shells feature a more isolated band of electrons that can respond to external light stimuli—an effect that has been previously observed with surface-confined nanotriangles with corner localized electromagnetic fields or "hot spots" that are shown to be highly optically sensitive [36, 42].

Unlike the optical enhancements observed with the NM-embedded films, there are no corresponding electrochemical effects observed in films with the NMs inserted close to the electrode, regardless of the type of NMs used. Electrochemical effects are, however, observed dependent on the location of the embedded NMs. That is, if the NMs are embedded at the solution–film interface, we observe a significant increase in Faradaic current of voltammetry for a solution redox probe-like $Fe(CN)_6^{3-/4-}$. This effect is observed with most of the NMs studied in this report, and it is speculated that their ability to enhance the current is directly related to their electronic coupling with the film, a phenomena that has been shown to be relevant in these types of assemblies [2]. Our results also highlight the extreme importance of electrostatic interactions both within these PEM films and at their interface, interactions that are clearly overridden with the addition of the NMs as the terminal layer of the films. It is evident from our study that the addition of specific NMs, strategically placed within PEM films, allows one to target either optical or electrochemical responses that are enhanced by the NMs and optimize the ability of these thin films to act as sensing materials.

Acknowledgements We gratefully acknowledge the National Science Foundation (CHE-0847145) and the Henry Dreyfus Teacher-Scholar Awards Program for generously supporting this research. We would like to specifically recognize Natalie Nguyen, Michael Freeman, and Debbie Campbell-Rance for their help with this project. Special thanks is given to Drs. T. Leopold, R. Kanters, D. Kellogg, R. Miller, and W. Case, as well as, Russ Collins, Phil Joseph, Mandy Mallory and John Wimbush—all of whom make undergraduate research possible at the University of Richmond. A very personal thank you is given to Kelsey Caroline Leopold.

References

1. Galyean AA, Day RW, Malinowski J, Kittredge KW, Leopold MC (2009) J Colloid Interface Sci 331:532
2. Dowdy CE, Leopold MC (2010) Thin Solid Films 519:790
3. Sun Y, Xia Y (2002) Anal Chem 74:5297
4. Malinsky MD, Kelly KL, Schatz GC, Van Duyne RP (2001) J Am Chem Soc 123:1471
5. Wang H, Brandl DW, Nordlander P, Halas NJ (2007) Acc Chem Res 40:53
6. Stewart ME, Anderton CR, Thompson LB, Maria J, Gray SK, Rogers JA, Nuzzo RG (2008) Chem Rev 108:494
7. Loftus AF, Reighard KP, Kapourales SA, Leopold MC (2008) J Am Chem Soc 130:1649
8. Yanez-Sedeno P, Pingarron JM (2005) Anal Bioanal Chem 382:884
9. Zhao J, Bradbury CR, Huclova S, Potapova I, Carrara M, Fermin DJ (2005) J Phys Chem B 109:22985
10. Jackson JB, Halas NJ (2001) J Phys Chem B 105:2743
11. Sun Y, Mayers BT, Xia Y (2002) Nano Lett 2:481
12. Westcott SL, Oldenburg SJ, Lee TR, Halas NJ (1999) Chem Phys Lett 300:651
13. Vargo ML, Gulka CP, Gerig JK, Manieri CM, Dattelbaum JD, Marks CB, Lawrence NT, Trawick ML, Leopold MC (2010) Langmuir 26:560
14. Doan TT, Vargo ML, Gerig JK, Gulka CP, Trawick ML, Dattelbaum JD, Leopold MC (2010) J Colloid Interface Sci 352:50
15. Schmitt J, Decher G, Dressick WJ, Brandow SL, Geer RE, Shashidhar R, Calvert JM (1997) Adv Mater 9:61
16. Isaacs SR, Choo H, Ko W-, Shon Y- (2006) Chem Mater 18:107
17. Jeon J, Panchagnula V, Pan J, Dobrynin AV (2006) Langmuir 22:4629
18. Vaskevich A, Rubinstein I (2007) Handbook of biosensors and biochips. Wiley, Chichester
19. Bradbury CR, Zhao J, Fermin DJ (2008) J Phys Chem C 112: 10153
20. Zhao J, Bradbury CR, Fermin DJ (2008) J Phys Chem C 112: 6832
21. Decher G, Hong JD, Schmitt J (1992) Thin Solid Films 210–211:831
22. Hicks JF, Young S, Murray RW (2002) Langmuir 18:2288
23. Musick MD, Keating CD, Keefe MH, Natan MJ (1997) Chem Mater 9:1499
24. Lyon LA, Pena DJ, Natan MJ (1999) J Phys Chem B 103:5826
25. Musick MD, Keating CD, Lyon LA, Botsko SL, Pena DJ, Holliway WD, McEvoy TM, Richardson JN, Natan MJ (2000) Chem Mater 12:2869
26. Lin S, Tsai Y, Chen C, Lin C, Chen C (2004) J Phys Chem B 108:2134
27. Russell LE, Galyean AA, Notte SM, Leopold MC (2007) Langmuir 23:7466
28. Silvert P, Herrera-Urbina R, Tekaia-Elhsissen K (1997) J Mater Chem 7:293
29. Brust M, Walker M, Bethell D, Schriffrin DJ, Whyman RJ (1994) J Chem Soc Chem Commun 801
30. Templeton AC, Wuelfing WP, Murray RW (2000) Acc Chem Res 33:27
31. Ingram RS, Hostetler MJ, Murray RW (1997) J Am Chem Soc 119:9175
32. Collinson M, Bowden EF, Tarlov MJ (1992) Langmuir 8:1247

33. Grabar KC, Smith PC, Musick MD, Davis JA, Walter DG, Jackson MA, Guthrie AP, Natan MJ (1996) J Am Chem Soc 118: 1148
34. Hoogvliet JC, Dijksma M, Kamp B, van Bennekom WP (2000) Anal Chem 72:2016
35. Russell LE, Pompano RR, Kittredge KW, Leopold MC (2007) J Mater Sci 42:7100. doi:10.1007/s10853-007-1545-6
36. Haes AJ, Zou S, Schatz GC, Van Duyne RP (2004) J Phys Chem B 108:6961
37. Mulvaney P (1996) Langmuir 12:788
38. Glenn JDH, Bowden EF (1996) Chem Lett 25:399
39. Finklea HO (1996) Electroanal Chem 19:109
40. Shiratori SS, Rubner MF (2000) Macromolecules 33:4213
41. Yoo D, Shiratori SS, Rubner MF (1998) Macromolecules 31: 4309
42. Zhao J, Das A, Zhang X, Schatz GC, Sligar SG, Van Duyne RP (2006) J Am Chem Soc 128:11004